THE NUCLEAR PHYSICS OF NEUTRON STARS*

J. Piekarewicz, R. Utama

Department of Physics, Florida State University
Tallahassee, FL 32306, USA

(Received December 18, 2015)

How Does Subatomic Matter Organize Itself? With their enormous dynamic range in density and neutron–proton asymmetry, neutron stars provide unique laboratories to answer this challenging question. Indeed, a neutron star is a gold mine for the study of physical phenomena that cut across a variety of disciplines, ranging from elementary particle physics to general relativity. Although the most common perception of a neutron star is that of a uniform assembly of neutrons packed to enormous densities, the reality is far different and much more interesting. In this contribution, we will focus on the dynamics of neutron-rich matter with special emphasis on its impact on the structure and composition of the outer crust. In particular, we will discuss a novel method that combines modern theoretical approaches with Bayesian Neural Networks to build a new mass formula that is then used to compute the crustal composition.

DOI:10.5506/APhysPolB.47.659

1. Introduction

One century ago, on December 2, 1915, Albert Einstein published his landmark paper on "Die Feldgleichungen der Gravitation" ("The Field Equations of Gravitation"). Almost two decades later, in an experiment that had no connections with the laws of gravitation, Chadwick would discover the neutron [1]. Very soon after Chadwick's announcement, the term *neutron star* appears in writing for the first time in the 1933 proceedings of the American Physical Society by Baade and Zwicky who wrote: *With all reserve we advance the view that supernovae represent the transition from ordinary stars into "neutron stars", which in their final stages consist of extremely closed packed neutrons* [2]. It appears, however, that a couple of years earlier Landau speculated on the existence of dense stars that look like giant

* Presented at the XXXIV Mazurian Lakes Conference on Physics, Piaski, Poland, September 6–13, 2015.

atomic nuclei. For an in-depth and fascinating tale on Landau's role on the possible existence of neutron stars see, Ref. [3]. Adopting the view espoused by Baade and Zwicky, Oppenheimer and Volkoff perform the first calculation of the structure of neutron stars by employing the full power of Einstein's theory of general relativity [4]. Using what it is now commonly referred to as the Tolman–Volkoff–Oppenheimer (TOV) equations [4, 5], Oppenheimer and Volkoff demonstrated that a neutron star supported exclusively by the quantum mechanical pressure from its degenerate neutrons will collapse into a black hole once its mass exceeds seven tenths of a solar mass. Seventy five years after such a pioneering prediction, the existence of neutron stars with masses as large as two solar masses has been firmly established [6, 7]. This fact alone highlights the vital role that nuclear interactions play in explaining the structure of neutron stars. Indeed, it is the repulsive character of the nucleon–nucleon interaction at short distances that provides the added pressure required to support a two-solar mass neutron star against gravitational collapse. This realization has created a powerful synergy between nuclear physics and astrophysics. Moreover, as we articulate below, a neutron star is a unique celestial laboratory for the study of nuclear phenomena over an enormous range of densities and neutron–proton asymmetries.

Although it is fairly well-understood how the number of electrons determines the chemistry of the atom and how this chemistry is responsible for binding atoms into molecules and molecules into both traditional and fascinating new materials, one would like to understand *how does matter organize itself* at densities significantly higher than those found in everyday materials; say, from 10^4–$10^{15}\,\mathrm{g/cm^3}$ (in this units nuclear-matter saturation density equals $2.48 \times 10^{14}\,\mathrm{g/cm^3}$). Indeed, relative to every day phenomena, these densities are so high that atoms become not thermal, but rather, pressure ionized. Understanding what novels phases of matter emerge under these extreme conditions of density is both fascinating and unknown. Moreover, it represents one of the grand challenges in nuclear physics. Remarkably, most of these exotic phases — *Coulomb crystals, nuclear pasta, color superconductors* — cannot be realized under normal laboratory conditions. It is gravity that leads to the stabilization of these novel states of matter. In this manner, neutron stars become the catalyst for the formation of unique states of matter and provide unique laboratories for the characterization of the ground state of cold matter over an enormous range of densities. Recall that a neutron star is not bound by the strong force but rather by gravity. Indeed, the typical gravitational binding energy per nucleon in a neutron star is about 100 MeV; this is more than ten times larger than the characteristic nuclear binding energy of 8 MeV per nucleon.

We have organized the paper as follows. In Sec. 2, we take a brief tour of a neutron star in order to appreciate its enormous diversity and dynamic range. After this brief journey into the neutron star, we provide in Sec. 3 a detailed account of the relatively simple physics that determines the composition of the outer crust and establish the predominant role played by the masses of a variety of exotic nuclei. In this section, particular emphasis is placed on a novel method that incorporated Bayesian Neural Networks (BNN) in the refinement of existing mass formulae. In turn, we use this newly-created mass formula in Sec. 4 to predict the crustal composition of a "canonical" neutron star. Finally, we conclude in Sec. 5.

2. Neutron-star structure

To appreciate the enormous dynamic range and richness displayed by these fascinating objects, we discuss briefly the anatomy of a neutron star. For a fairly accurate rendition of the structure and phases of a neutron star, see Figs. 1 and 2. Neutron stars contain a non-uniform crust above

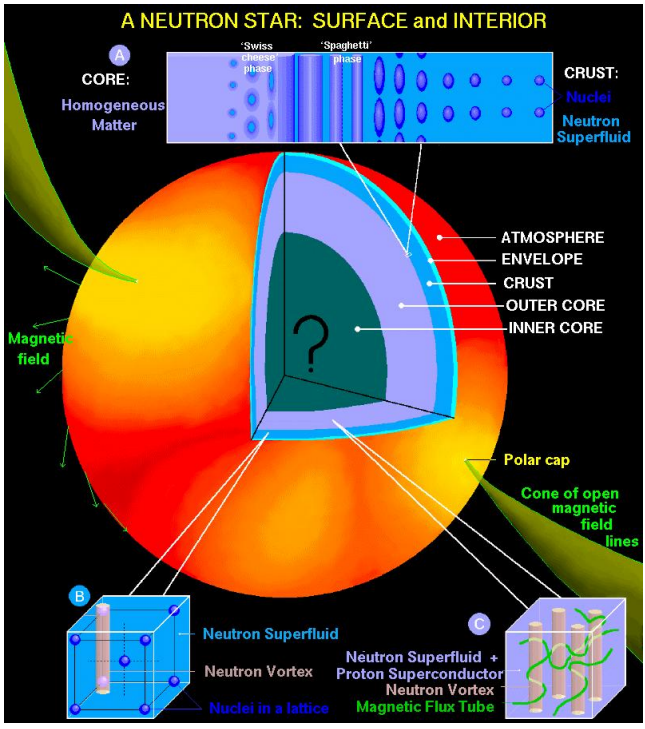

Fig. 1. An accurate rendition of the fascinating structure and exotic phases that are believed to exist in a neutron star — courtesy of Dany Page.

a uniform liquid core that is comprised of a uniform assembly of neutrons, protons, electrons, and muons in chemical equilibrium and packed to densities that may exceed that of normal nuclei by up to an order of magnitude. The highest density attained in the stellar core depends critically on the equation of state of neutron-rich matter, which at those high densities is poorly constrained. However, for soft equations of state, namely, those with a pressure that rises slowly with density, the highest density attained at the core may be high enough for the emergence of new exotic phases, such as pion or kaon condensates [8, 9], strange quark matter [10], and color superconductors [11, 12].

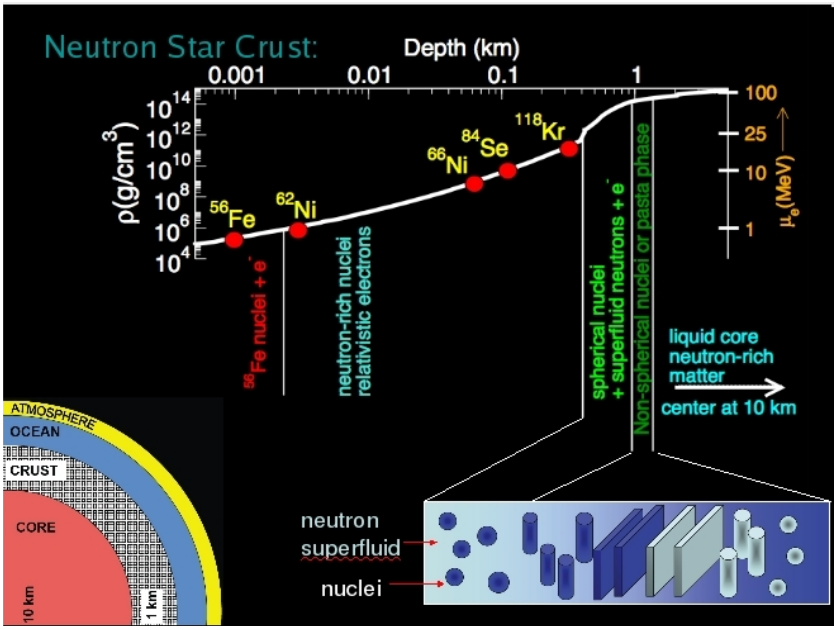

Fig. 2. An accurate depiction of the assumed composition of the crust of a neutron star — courtesy of Sanjay Reddy.

At the other extreme, namely, at densities of about half of nuclear-matter saturation density, the uniform core becomes unstable against cluster formation. At these "low" densities, the average inter-nucleon separation increases to such an extent that it becomes energetically favorable for the system to segregate into regions of normal density (nuclear clusters) and regions of low density (dilute, likely superfluid, neutron vapor). Such a clustering instability signals the transition from the uniform liquid core to the non-uniform crust. The solid crust is itself divided into an outer and an inner region. The outer crust spans a region of about seven orders of magnitude in density; from about 10^4 g/cm^3 to 4×10^{11} g/cm^3 [13–18]. Structurally, the outer crust

is comprised of a Coulomb lattice of neutron-rich nuclei embedded in a uniform electron gas. As the density increases — and given that the electronic Fermi energy increases rapidly with density — it becomes energetically favorable for electrons to capture into protons. This results in the formation of Coulomb crystals of progressively more neutron-rich nuclei. This progression starts with ^{56}Fe — the nucleus with the lowest mass per nucleon — and is predicted to end with the exotic, neutron-rich nucleus ^{118}Kr (see Fig. 2). In essence, the most stable nucleus at a given crustal density emerges from a competition between the electronic Fermi energy (which favors low Z) and the nuclear symmetry energy (which favors $N \simeq Z$ nuclei) [17, 18]. Eventually, however, the neutron–proton asymmetry becomes too large for the nuclei to absorb any more neutrons and the excess neutrons form of a dilute — likely superfluid — neutron vapor; this signals the transition from the outer to the inner crust. At a *neutron-drip* density of about 4×10^{11} g/cm^3, ^{118}Kr is unable to retain any more neutrons. As alluded earlier, at densities approaching nuclear-matter saturation density ($\approx 2.5 \times 10^{14}$ g/cm^3) uniformity in the system will be restored. Yet the transition from the highly-ordered crystal to the uniform liquid is both interesting and complex. This is because distance scales that were well-separated in both the crystalline phase (where the long-range Coulomb interaction dominates) and in the uniform phase (where the short-range strong interaction dominates) become comparable. This unique situation gives rise to *Coulomb frustration*. Frustration, a phenomenon characterized by the existence of a very large number of low-energy configurations, emerges from the impossibility to simultaneously minimize all elementary interactions in the system. Indeed, as these length scales become comparable, competition among the elementary interactions results in the formation of a myriad of complex structures radically different in topology yet extremely close in energy. Given that these complex structures — collectively referred to as *nuclear pasta* — are very close in energy, it has been speculated that the transition from the highly ordered crystal to the uniform phase must proceed through a series of changes in the dimensionality and topology of these structures [19, 20]. Moreover, due to the preponderance of low-energy states, frustrated systems display an interesting and unique low-energy dynamics that has been captured using a variety of techniques including numerical simulations [21–29] with some of the most recent ones involving an enormous number of nucleons. Whereas these impressive numerical simulations predict the development of unique many-body correlations from a relatively simple underlying nucleon–nucleon interaction, they miss potentially important quantum effects. In this context, the structure of the inner stellar crust has been investigated for over 15 years using a fully quantum approach that, in particular, illustrates the emergence of shell effects in the neutron vapor surrounding the heavy clus-

ters [30–34] — an effect that is impossible to capture in the (semi-classical) numerical simulations. Of course, given that most of the quantum effects are incorporated at the mean-field level, quantum calculations miss some of the many-body correlations that emerge in the numerical simulations. However, this has created a unique synergy between the two complementary approaches that has confirmed that the development of the nuclear pasta is robust under the conditions present in the inner stellar crust.

3. The outer crust: sensitivity to nuclear masses

As described earlier, at the very low densities of the outer crust, it becomes energetically favorable for nucleons to cluster into nuclei that arrange themselves in a crystalline structure embedded in a neutralizing electron background. Because of limitations in space — and due to recent developments in the improvement of mass models — we will concentrate in this contribution exclusively on the structure and composition of the outer stellar crust.

The dynamics of the outer crust is encapsulated in a relatively simple expression for the total Gibbs free energy per nucleon, which at zero temperature equals the total chemical potential of the system. That is [14–18],

$$\mu(Z,A;P) = \frac{M(Z,A)}{A} + \frac{Z}{A}\mu_e - \frac{4}{3}C_{\rm l}\frac{Z^2}{A^{4/3}}\,p_{\rm F}\,. \tag{1}$$

The first term is independent of the pressure — or equivalently of the baryon density $n = A/V$ — and represents the entire nuclear contribution to the chemical potential. It depends exclusively on the mass per nucleon of the "optimal" nucleus populating the crystal lattice. The second term represents the electronic contribution from the relativistic electrons. Finally, the last term provides the relatively modest — although by no means negligible — electrostatic lattice contribution (with $C_{\rm l} = 3.40665 \times 10^{-3}$). Here, $p_{\rm F}$ is the nuclear Fermi energy that is related to the baryon density through the following expression

$$p_{\rm F} = \left(3\pi^2 n\right)^{1/3}\,. \tag{2}$$

The connection between the pressure and the baryon density is provided by the underlying crustal equation of state that is dominated by the relativistic electrons. That is,

$$P(Z,A;n) = \frac{m_e^4}{3\pi^2}\left(x_{\rm F}^3 y_{\rm F} - \frac{3}{8}\left[x_{\rm F}y_{\rm F}\left(x_{\rm F}^2+y_{\rm F}^2\right) - \ln(x_{\rm F}+y_{\rm F})\right]\right) - \frac{n}{3}C_{\rm l}\frac{Z^2}{A^{4/3}}\,p_{\rm F}\,, \tag{3}$$

where $x_{\rm F} = p_{\rm F}^e/m_e$ and $y_{\rm F} = (1+x_{\rm F}^2)^{1/2}$ are scaled electronic Fermi momentum and Fermi energy, respectively and with $p_{\rm F}^e = (Z/A)^{1/3}p_{\rm F}$. This discussion suggests that the only unknown in the determination of the crustal composition is the optimal nucleus, namely, the one that minimizes the chemical potential at a given pressure.

The search for the optimal nucleus is performed as follows. For a given pressure P and nuclear species (Z, A), the equation of state is used to determine the corresponding baryon density of the system which, in turn, determines the Fermi momentum $p_{\rm F}$ and the electronic chemical potential μ_e. This is sufficient to compute the chemical potential of the system as indicated in Eq. (1). This procedure requires scanning over an entire mass table — which in some instances consists of nearly 10,000 nuclei. The (Z, A) combination that minimizes $\mu(A, Z; P)$ determines the optimal nucleus at the given pressure. Naturally, if the density is very small so that the electronic contribution to the chemical potential is negligible, then ^{56}Fe — with the lowest mass per nucleon — becomes the nucleus of choice. As the pressure and density increase so that the electronic contribution may no longer be neglected, then it becomes advantageous to reduce the electron fraction Z/A at the expense of increasing the neutron–proton asymmetry. In turn, this results in an increase in the mass per nucleon. Which nucleus becomes the optimal choice then emerges from a subtle competition between the electronic contribution that favors $Z = 0$, and the nuclear symmetry energy which favors (nearly) symmetric nuclei.

In summary, the structure of the outer stellar crust consists of a nuclear lattice embedded in an electron gas that is responsible for driving the system towards progressively more neutron-rich nuclei. In this way, the outer crust represents a unique laboratory for the study of neutron-rich nuclei in the $Z \simeq 20$–50 region that nicely complements our quest for a detailed map of the nuclear landscape at terrestrial laboratories. In the following section, we introduce the BNN approach that will be used to predict the masses of the nuclei (some of them highly exotic) that populate the outer crust [35].

3.1. Density functional theory meets Bayesian Neural Networks

Quantum Chromodynamics (QCD) is widely regarded as the fundamental theory of the strong interaction. However, the complexity of QCD presents enormous challenges in solving the theory in the non-perturbative regime of relevance to nuclear systems. Although inspired by QCD, to date the description of the nuclear dynamics relies on effective theories using appropriate degrees of freedom, such as nucleons and mesons. Among the effective approaches, *density functional theory* (DFT) is the most promising — and perhaps unique — microscopic approach that may be applied

to both finite nuclei and neutrons stars — objects that differ in size by 18 orders of magnitude! In the past decades, enormous progress has been made in building sophisticated nuclear *energy density functionals* (EDFs) of both non-relativistic [36–39] and relativistic character [40–45]. Besides relying on some more sophisticated fitting protocols, some of the most recent EDFs provide full uncertainty quantification. However, in spite of such enormous gains, one must recognize that these effective theories are, at best, approximations to QCD. Moreover, whereas model predictions tend to agree near stability, they are often in stark disagreement far away from their region of applicability [46]. Based on these inevitable facts, we propose a novel approach that starts with the construction of an accurately-calibrated EDF that incorporates as much physics as possible in both the quality of the functional and the set of observables used to constrain the fit. However, once the calibration is completed, one transfers control to a proven sophisticated numerical algorithm to perform a fine tuning. We propose to perform the fine tuning by using *Bayesian Neural Networks*. The BNN approach is predicated on the existence of a "universal approximator" that is capable of approximating any real function of one or more real variables [47, 48]. The utility of the Bayesian approach to neural-network optimization is that it furnishes an estimate of the uncertainty in the approximated function in a computationally convenient manner. Although in this contribution we illustrate the approach for the important case of nuclear masses, it should be underscored that it may be easily extended to any other nuclear observable.

The proposed method starts by computing nuclear masses over the entire nuclear chart using modern relativistic energy density functionals. In the spirit of Strutinsky's energy theorem [49], we may regard these mass predictions as providing the large and "smooth" contribution of the underlying mass function $M_{\rm DFT}(Z,N)$. The next step consists of a refinement of the mass model by "training" a suitable neural network on the *mass residuals*; that is, on the difference between the (imperfect) predictions of the mass models and experiment. Once properly trained, we used the resulting "universal approximator" $\delta_{\rm LDM}(Z,N)$ (a) to validate the approach and (b) to make predictions in regions where experimental information is presently unavailable. That is, the resulting mass formula becomes equal to

$$M(Z,N) \equiv M_{\rm DFT}(Z,N) + \delta_{\rm BNN}(Z,N)\,. \tag{4}$$

Given that both the predictions of $M_{\rm DFT}$ and of the residuals $\delta_{\rm BNN}$ involve the calibration of an objective function, all mass predictions are accompanied by properly estimated theoretical errors.

4. Results: The composition of the outer crust

To illustrate the power of the BNN refinement, we display in Fig. 3 theoretical predictions for the masses of the four exotic ^{102}Kr, ^{105}Kr, ^{108}Kr, and ^{111}Kr isotopes where experimental information is not yet available. The figure includes predictions for all these four isotopes from a representative set of successful mass models. These include the microscopic–macroscopic mass models of Duflo and Zuker (DZ) [50] and the finite range droplet model (FRDM) of Möller and collaborators [51] — as well as the two accurately-calibrated microscopic models HFB19 and HFB21 [36]. Given the lack of experimental data, results are displayed relative to the predictions of Duflo and Zuker. Note that these predictions are depicted in the figure *without* theoretical error bars. As expected, we observe a significant spread in the model predictions when experimental data is not available (for a dramatic depiction of this effect, see Fig. 42 in Ref. [46]). However, once the BNN refinement is implemented, most of these systematic differences disappear. Moreover, because the determination of the universal approximator is implemented through a Monte Carlo approach, all mass predictions now contain a proper quantification of the theoretical uncertainties. Ultimately, one can then compute a "world average" value by combining the BNN-improved predictions. In this manner, a "BNN-world" mass table has been created [35]. Such a mass table will now serve to predict the composition of the outer crust of a neutron star by implementing the procedure described in Sec. 3.

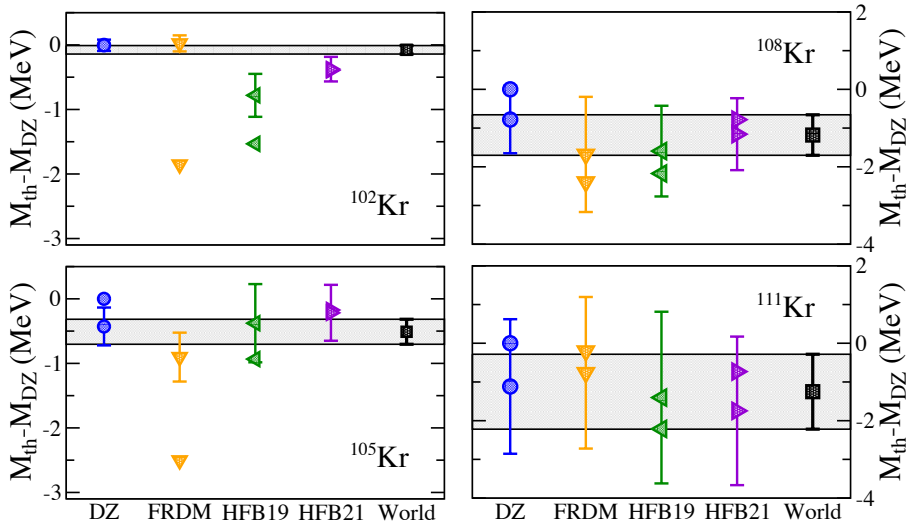

Fig. 3. Pre- and post-BNN improved mass predictions relative to the "bare" Duflo–Zuker values for ^{102}Kr, ^{105}Kr, ^{108}Kr, and ^{111}Kr. The BNN predictions include statistical errors and "World" represents the world average of the four models.

Once a mass table is constructed, we can identify the nuclear species that minimizes the total chemical potential given in Eq. (1) as a function of the pressure. The outcome of this procedure is displayed in Fig. 4 where the composition of the outer crust as a function of depth is obtained for a "canonical" $1.4\,M_\odot$ neutron star with an assumed radius of 12.78 km. Once the mass and radius of the neutron star has been selected, the crustal composition as a function of depth may be obtained from integrating *inwards* the Tolman–Oppenheimer–Volkoff equations. Predictions for the crustal composition are shown using three mass models: the newly created "BNN-world", Duflo–Zuker, and HFB19 — the last two without any BNN refinement. The composition of the upper layers of the crust where the pressure and density are low — depicted in light gray/yellow and spanning about 100 m — consists of Fe–Ni nuclei with masses that are well-known experimentally. As the Ni-isotopes become progressively more neutron rich as a consequence of an increase in density, it becomes energetically favorable to transition into the magic $N = 50$ isotone region. In the particular case of BNN-world, this intermediate region is predicted to start with stable ^{86}Kr and then progressively evolve into the more exotic isotones ^{84}Se ($Z = 34$), ^{82}Ge ($Z = 32$), ^{80}Zn ($Z = 30$), and ^{78}Ni ($Z = 28$). In this region, most of the masses are experimentally known, although for some of them the quoted value is not derived from purely experimental data [52]. Note, in particular, that the newly created BNN-world model predicts a binding energy per nucleon for the doubly magic ^{78}Ni nucleus of $B/A = 8232.412(390)$ keV. Ultimately, at

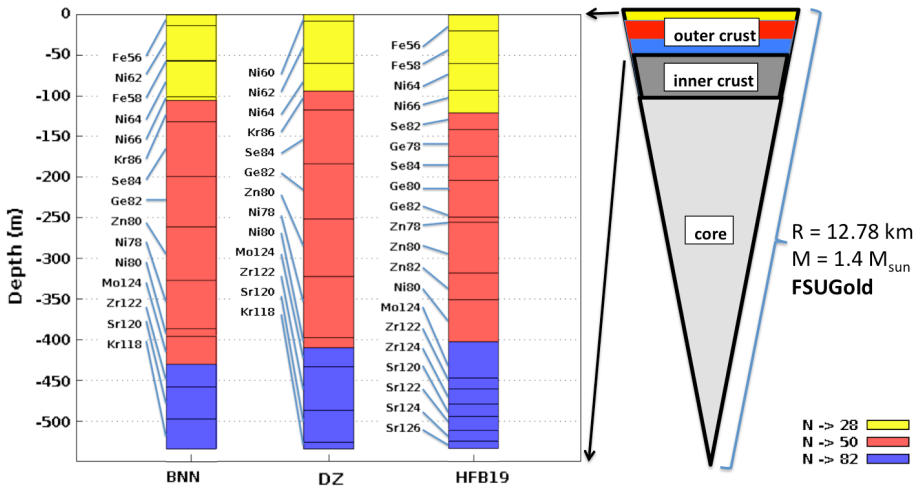

Fig. 4. Composition of a canonical $1.4\,M_\odot$ neutron star with a 12.78 km radius as predicted by three mass models: "BNN-world", DZ, and HFB19.

the highest densities encountered in the outer crust, it becomes energetically favorable for the system to transition into the magic $N = 82$ isotone region. In this region, *none of the relevant nuclei have experimentally determined masses*. Although not shown, it is interesting to note that the composition of the HFB19 model changes considerably after the BNN refinement, bringing it into closer agreement with the predictions of both the BNN-world and Duflo–Zuker models.

5. Conclusions

Neutron stars provide a powerful intellectual bridge between nuclear physics and astrophysics. In this contribution, we explored the fascinating structure of neutron stars and established the prominent role that nuclear physics plays in elucidating the underlying physics. In the particular case of the outer crust, we established the fundamental role that mass measurements of exotic nuclei at rare isotope facilities will play in elucidating its unique composition.

Given that the composition of the neutron star crust — as well as r-process nucleosynthesis — demands knowledge of nuclear masses far away from stability, we introduced a novel approach that combines modern density functional theory with Bayesian neural networks. Whereas density functional theory provides the most powerful theoretical framework to compute nuclear properties throughout the nuclear chart, large systematic uncertainties among the various models hinder the interpretation of both experimental and observational data. Moreover, these uncertainties grow to unacceptable levels when predictions are made in regions of the nuclear chart where experimental data is unavailable. The addition of the BNN approach was able to overcome some of these limitations and provided the necessary fine tuning to account for the small deviations from experiment. Most importantly, the spread in the predictions of the various mass models was considerable reduced. Finally, due to its inherent probabilistic nature, the Bayesian approach provided improved mass predictions with proper theoretical errors.

As a first test of the new mass model, we have computed the exotic composition of the outer crust of a neutron star. Suffice it to say that none of the exotic nuclei that are predicted to inhabit the bottom layers of the outer crust have been measured. And while this situation is likely to persist for many years to come, it is still essential to continue the experimental exploration of the nuclear chart in an effort to inform theory. Finally, we conclude by underscoring that a precise knowledge of the crustal composition is vital in the study of certain elastic properties of the crust, such as its shear modulus and breaking strain — quantities that are of great relevance to magnetar starquakes [53, 54] and gravitational wave emission [55].

This material is based upon work supported by the U.S. Department of Energy Office of Science, Office of Nuclear Physics under Award Number DE-FD05-92ER40750.

REFERENCES

[1] J. Chadwick, *Nature* **129**, 312 (1932).
[2] W. Baade, F. Zwicky, *Phys. Rev.* **45**, 138 (1934).
[3] D.G. Yakovlev, P. Haensel, G. Baym, C.J. Pethick, *Phys. Usp.* **56**, 289 (2013).
[4] J.R. Oppenheimer, G.M. Volkoff, *Phys. Rev.* **55**, 374 (1939).
[5] R.C. Tolman, *Phys. Rev.* **55**, 364 (1939).
[6] P. Demorest *et al.*, *Nature* **467**, 1081 (2010).
[7] J. Antoniadis *et al.*, *Science* **340**, 6131 (2013).
[8] P.J. Ellis, R. Knorren, M. Prakash, *Phys. Lett. B* **349**, 11 (1995).
[9] J.A. Pons, J.A. Miralles, M. Prakash, J.M. Lattimer, *Astrophys. J.* **553**, 382 (2001).
[10] F. Weber, *Prog. Part. Nucl. Phys.* **54**, 193 (2005).
[11] M.G. Alford, K. Rajagopal, F. Wilczek, *Nucl. Phys. B* **537**, 443 (1999).
[12] M.G. Alford, A. Schmitt, K. Rajagopal, T. Schafer, *Rev. Mod. Phys.* **80**, 1455 (2008).
[13] G. Baym, C. Pethick, P. Sutherland, *Astrophys. J.* **170**, 299 (1971).
[14] P. Haensel, J.L. Zdunik, J. Dobaczewski, *Astron. Astrophys.* **222**, 353 (1989).
[15] P. Haensel, B. Pichon, *Astron. Astrophys.* **283**, 313 (1994).
[16] S.B. Ruester, M. Hempel, J. Schaffner-Bielich, *Phys. Rev. C* **73**, 035804 (2006).
[17] X. Roca-Maza, J. Piekarewicz, *Phys. Rev. C* **78**, 025807 (2008).
[18] X. Roca-Maza, J. Piekarewicz, T. Garcia-Galvez, M. Centelles, in: *Neutron Star Crust*, C. Bertulani, J. Piekarewicz (Eds.), New York, Nova Publishers, 2011.
[19] D.G. Ravenhall, C.J. Pethick, J.R. Wilson, *Phys. Rev. Lett.* **50**, 2066 (1983).
[20] M. Hashimoto, H. Seki, M. Yamada, *Prog. Theor. Phys.* **71**, 320 (1984).
[21] C.J. Horowitz, M.A. Perez-Garcia, J. Piekarewicz, *Phys. Rev. C* **69**, 045804 (2004).
[22] C.J. Horowitz *et al.*, *Phys. Rev. C* **70**, 065806 (2004).
[23] C.J. Horowitz, M.A. Perez-Garcia, D.K. Berry, J. Piekarewicz, *Phys. Rev. C* **72**, 035801 (2005).
[24] G. Watanabe, K. Sato, K. Yasuoka, T. Ebisuzaki, *Phys. Rev. C* **68**, 035806 (2003).
[25] G. Watanabe *et al.*, *Phys. Rev. Lett.* **94**, 031101 (2005).

[26] G. Watanabe *et al.*, *Phys. Rev. Lett.* **103**, 121101 (2009).
[27] A. Schneider, C. Horowitz, J. Hughto, D. Berry, *Phys. Rev. C* **88**, 065807 (2013).
[28] C.J. Horowitz *et al.*, *Phys. Rev. Lett.* **114**, 031102 (2015).
[29] M.E. Caplan, A.S. Schneider, C.J. Horowitz, D.K. Berry, *Phys. Rev. C* **91**, 065802 (2015).
[30] A. Bulgac, P. Magierski, *Nucl. Phys. A* **683**, 695 (2001).
[31] P. Magierski, P.-H. Heenen, *Phys. Rev. C* **65**, 045804 (2002).
[32] N. Chamel, *Nucl. Phys. A* **747**, 109 (2005).
[33] W. Newton, J. Stone, *Phys. Rev. C* **79**, 055801 (2009).
[34] B. Schuetrumpf, W. Nazarewicz, *Phys. Rev. C* **92**, 045806 (2015).
[35] R. Utama, J. Piekarewicz, H.B. Prosper, *Phys. Rev. C* **93**, 014311 (2016).
[36] S. Goriely, N. Chamel, J. Pearson, *Phys. Rev. C* **82**, 035804 (2010).
[37] M. Kortelainen *et al.*, *Phys. Rev. C* **82**, 024313 (2010).
[38] J. Erler *et al.*, *Phys. Rev. C* **87**, 044320 (2013).
[39] M. Kortelainen *et al.*, *JPS Conf. Proc.* **6**, 020018 (2015).
[40] G.A. Lalazissis, J. Konig, P. Ring, *Phys. Rev. C* **55**, 540 (1997).
[41] G.A. Lalazissis, S. Raman, P. Ring, *At. Data Nucl. Data Tables* **71**, 1 (1999).
[42] B.G. Todd-Rutel, J. Piekarewicz, *Phys. Rev. Lett.* **95**, 122501 (2005).
[43] F.J. Fattoyev, C.J. Horowitz, J. Piekarewicz, G. Shen, *Phys. Rev. C* **82**, 055803 (2010).
[44] W.-C. Chen, J. Piekarewicz, *Phys. Rev. C* **90**, 044305 (2014).
[45] W.-C. Chen, J. Piekarewicz, *Phys. Lett. B* **748**, 284 (2015).
[46] K. Blaum, *Phys. Rep.* **425**, 1 (2006).
[47] D.M. Titterington, *Statist. Sci.* **19**, 128 (2004).
[48] R.M. Neal, *Bayesian Learning of Neural Network*, Springer, New York 1996.
[49] V.M. Strutinsky, *Nucl. Phys. A* **95**, 420 (1967).
[50] J. Duflo, A. Zuker, *Phys. Rev. C* **52**, R23 (1995).
[51] P. Möller, J.R. Nix, W.D. Myers, W.J. Swiatecki, *Atom. Data Nucl. Data Tables* **59**, 185 (1995).
[52] M. Wang *et al.*, *Chin. Phys. C* **36**, 1603 (2012).
[53] A.L. Piro, *Astrophys. J.* **634**, L153 (2005).
[54] A.W. Steiner, A.L. Watts, *Phys. Rev. Lett.* **103**, 181101 (2009).
[55] C. Horowitz, K. Kadau, *Phys. Rev. Lett.* **102**, 191102 (2009).